Exploiting delayed transitions to sustain semiarid ecosystems after catastrophic shifts
Supporting Information
J. R. Soc. Interface

Blai Vidiella[1,2], Josep Sardanyés[3,4] , Ricard Solé[1,2,5,*]

1. ICREA-Complex Systems Lab, Department of Experimental and Health Sciences, Universitat Pompeu Fabra, Dr. Aiguader 88, 08003 Barcelona, Spain
2. Institut de Biologia Evolutiva (CSIC-Universitat Pompeu Fabra), Pg. Marítim de la Barceloneta 37, 08003 Barcelona, Spain
3. Centre de Recerca Matemàtica. Campus de Bellaterra, Edifici C 08193 Bellaterra, Barcelona, Spain
4. Barcelona Graduate School of Mathematics (BGSMath). Campus de Bellaterra, Edifici C 08193 Bellaterra, Barcelona, Spain
5. Santa Fe Institute, 1399 Hyde Park Road, Santa Fe, NM 87501, USA
* corresponding author

Contents

1. FIXED POINTS AND LINEAR STABILITY ANALYSIS

The mathematical model we are studying is given by the next couple of differential equations:

$$\begin{aligned} \dot{V} &= V\left((b-cV)\,S-m\right), \\ \dot{S} &= fV\left(1-S-V\right)-dS-V\left((b-cV)\,S-m\right). \end{aligned} \tag{1}$$

The state variables V and S denote the fractions of vegetation and fertile soil, respectively (see Section II in the main manuscript for the meaning of the parameters). The fixed points are obtained by setting the time derivatives $\dot{V}=0$ and $\dot{S}=0$ simultaneously. By doing so, we obtain a first fixed point, labeled $P_0^*=(0,0)$. The (linear) stability of a given fixed point, P^*, is obtained from $\det|\mathcal{J}(P^*)-\lambda I|=0$, $\mathcal{J}$ being the Jacobian matrix of Eqs. (1) and I being the identity matrix. Constants λ correspond to the eigenvalues, whose sign determine the stability. The Jacobian matrix reads:

$$\mathcal{J}(V,S)=\begin{pmatrix} S(b-2Vc)-m & V(b-cV) \\ f(1-S-2V)+S(2cV-b)+m & -V(f+b-cV)-d \end{pmatrix}.$$

The fixed point P_0^* is locally asymptotically stable since both eigenvalues are negative, with $\lambda_1(P_0^*)=-m$ and $\lambda_2(P_0^*)=-d$, with $m,d>0$. The calculation of the other fixed points is rather cumbersome due to the structure of the model. Alternatively, the biologically-meaningful fixed points can be found by means of the nullclines of Eqs. (1), defined as the curves where either $\dot{V}=0$ or $\dot{S}=0$, with:

$$\dot{V}=0 \qquad \rightarrow \qquad S(V)=\frac{m}{b-cV}, \tag{2}$$

$$\dot{S}=0 \qquad \rightarrow \qquad S(V)=\frac{V\left(f(1-V)-m\right)}{V(f+b-cV)+d}. \tag{3}$$

The intersections of these nullclines provide the equilibrium points of the system since $\dot{V}=\dot{S}=0$. Figure 1 displays the shape of these nullclines and how they change in terms of the parameter d. In Fig. 1a we set $d=0.1$, and both nullclines intersect twice inside the phase space. This scenario corresponds to bistability since two stable fixed points P_0^* and P_2^* are found, separated by an unstable one (named P_1^*). We notice that numerical solutions of Eqs. (1) as well as the

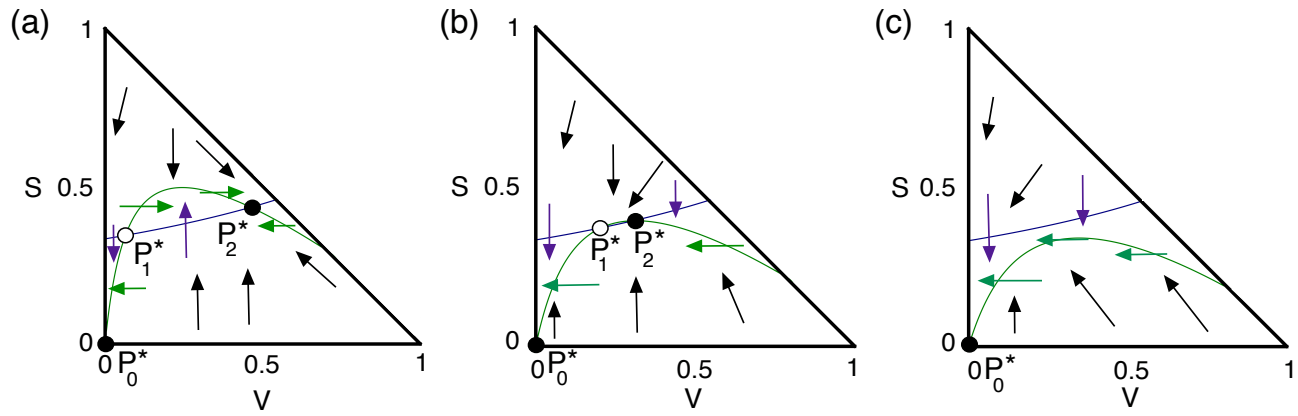

FIG. 1: Nullclines obtained from Eq. (2) (violet line) and Eq. (3) (green line). The directions of the flows are indicated with small arrows. Here the intersections of the nullclines are the fixed points (black: stable node; white: saddle). Three different dynamical scenarios for several values of the parameter d are displayed: (a) bistability with persistence of about 50% of the vegetation (given by the stable fixed point P_2^*), with $d = 0.1 < d_c$; (b) decrease of the fraction of vegetation and approach of the unstable fixed point P_1^* to P_2^*, with $d = 0.2104 \lesssim d_c$. Finally, in (c) we set $d = 0.32 > d_c$, and the fixed point involving the desert state P_0^* becomes globally asymptotically stable since both fixed points P_1^* and P_2^* have coalesced in a saddle-node bifurcation. In all of the panels we set $b = 0.3$, $c = 0.15$, $m = 0.1$, and $f = 0.9$.

pseudo-potential analysis (see Section 4 below) indicate that the fixed point P_2^* is an attractor (see also Figs. 1 and 2 in the main manuscript). As d increases towards its bifurcation value d_c, both fixed points P_1^* and P_2^* approach each other, as displayed in Fig. 1b. The value of d_c has been computed very accurately (see Section 2 below). At the bifurcation value, both fixed points P_1^* and P_2^* collide and disappear in a saddle-node bifurcation. Hence, for $d > d_c$, the only fixed point in the phase space is P_0^*, which becomes globally asymptotically stable (see Fig. 1c).

2. SHARP CALCULATION OF THE CRITICAL DEGRADATION RATE OF FERTILE SOIL

An accurate calculation of the bifurcation value of the degradation rate of fertile soil is a key point in our analyses since we are analyzing a phenomenon that occurs very near the saddle-node bifurcation. The bifurcation value can be usually calculated analytically from the expressions of the two fixed points involved in the saddle-node bifurcation: fixed points P_1^* and P_2^* in our system. When the fixed points can not be calculated analytically, other strategies can be followed. One possible way of obtaining a very sharp calculation of this bifurcation value is by means of the so-called double discriminant theory. Computing bifurcation values with high accuracy is usually an extra difficulty in many problems, requiring an important numerical computation effort. However, when the vector field is of polynomial type (like in our model) or even rational, algebraic tools can help us to find such values with more precision. The key point is to transform the original problem of looking for zeroes into a more simplified, well-posed one.

This method is based on the so-called *discriminant* and *resultants* of one or a pair of polynomials. Roughly speaking, modulo some suitable constant, it is the product of the differences of the roots of the polynomial, counted with their multiplicity. It is a symmetric function of them. Closely related to this, we have the definition of *resultant* of two polynomials, $\mathrm{Res}\,(p(x), q(x))$, defined as the product of the difference between the roots of p and the roots of q (counted again with their multiplicity). Therefore, $\mathrm{Res}\,(p, q) = 0$ if and only if $p(x)$ and $q(x)$ have a common root. The discriminant Δ of a polynomial $p(x)$ can be expressed as a constant multiplied by the $\mathrm{Res}\,(p(x), p'(x))$. Zeroes of the resultant (or the discriminant) determine in many situations a change in the topology or in the behaviour of the problem (related to the change in the number of zeroes of p).

This method, as mentioned, can be used in many biological models when the vector field is polynomial. This is the case of our problem, where the system has an expression of the form

$$\begin{cases} \dot{V} &= F(V,S), \\ \dot{S} &= G(V,S,d) - F(V,S), \end{cases}$$

where d is taken as the parameter governing the bifurcation analysis, and

$$F(V,S) = V\left((b - cV)\,S - m\right), \qquad G(V,S,d) = fV\,(1 - S - V) - dS.$$

The amount and behaviour of the equilibrium points is determined from the zeroes of the system

$$\begin{cases} F(V,S) &= 0, \\ G(V,S,d) &= 0, \end{cases}$$

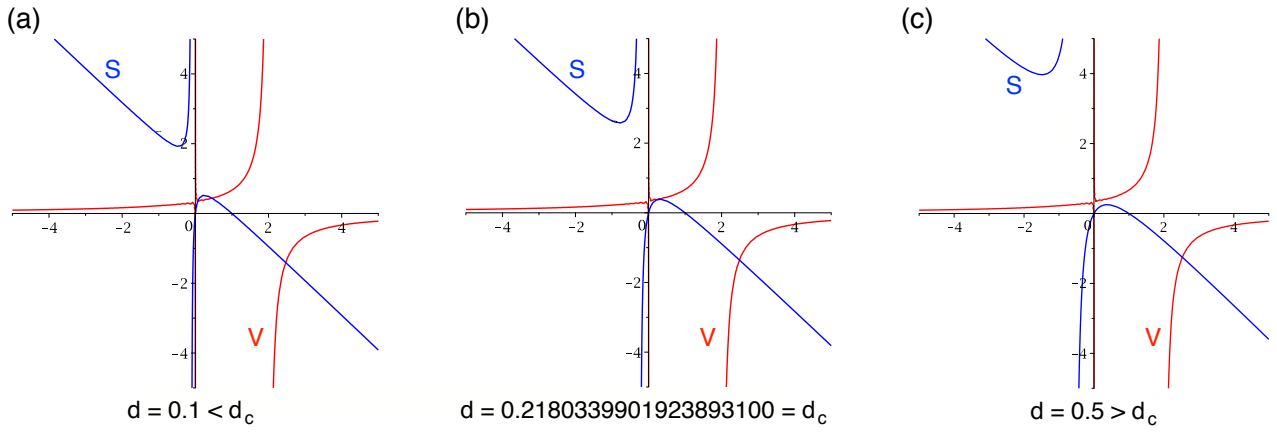

FIG. 2: Shape of the curves $F = 0$ and $G = 0$ below (a); at (b); and above (c) the bifurcation value (see Section 2). (a) The two curves intersect twice in the positive biologically-meaningful phase space below the bifurcation, here with $d = 0.1 < d_c$. (b) The curves F and G are tangent just at the bifurcation value $d = d_c$. (c) Above the bifurcation the two curves do not intersect between each other, here with $d = 0.5 > d_c$. In all of the panels we also set $b = 0.3$, $c = 0.15$, $m = 0.1$, and $f = 0.9$. The changes in the nullclines at increasing d can be seen in the animation file: movie1.gif.

that is, the intersection points between both nullclines. Since the polynomials F and G depend on two variables, the method used is an extension of the presented above. It is based on the computation of the so-called *double resonant* (see, for instance Niu and Wang 2008; García-Saldaña *et al.* 2014; García-Saldaña and Gasull 2015; and Ferragut *et al.* 2016 and references therein). Since we are interested in the bifurcation value of the degradation rate of fertile soil, given by parameter d, we will fix all other model parameters at the same values used throughout all the analyses of our manuscript. Specifically, we are interested in d_c when $b = 0.3$, $c = 0.15$, $m = 0.1$, and $f = 0.9$. The computations to get d_c, performed in `Maple`, consisted in the following steps:

- Computation of

$$\begin{aligned} R_S(V,d) = \mathrm{Res}(F,G,S) &= 0.1350000000\,V^4 - 0.4050000000\,V^3 + 0.1800000000\,V^2 \\ &\quad -0.09999999999\,dV, \end{aligned}$$

$$\begin{aligned} R_V(S,d) = \mathrm{Res}(F,G,S) &= 0.02250000000\,d^2S^4 + 0.0405000000\,dS^4 + 0.027000000\,dS^3 \\ &\quad -0.04050000000\,dS^2 + 0.009000000000\,dS. \end{aligned}$$

- We compute the resultants (the discriminant, modulo a constant):

$$\begin{aligned} R_{SV}(d) &= \mathrm{Res}(R_S(V), R_S'(V)) \\ &= -0.6643012494 \cdot 10^{-5}(d + 2.018033989)d^2(d - .2180339889) \end{aligned}$$

$$\begin{aligned} R_{VS}(d) &= \mathrm{Res}(R_V(S), R_V'(S)) \\ &= -2.017815047 \cdot 10^{-12}\ (d + 2.01803397821724184)\,(d + 1.80000001187603065) \\ &\quad \cdot d^7\,(d - 0.218033990192389310)\,. \end{aligned}$$

- Finally, the true (real) bifurcation values to consider are those common roots of these two last polynomials. In our case, since the paramater d must be non-negative, this is easily computed and provides the values $d_1 = 0$ and $d_2 = 0.21803399019238931000 = d_c$.

It is straigthforward to check that for values of d in $d_1 \leq d < d_2$ there are three transversal intersections between the curves $F = 0$ and $G = 0$ (indicating the scenario of bistability); at $d = d_1$ just two (one of them tangential); and for $d > d_1$ one transversal intersection (see Fig. 2, and movie1.gif in the online material for an animation about how the curves evolve at growing d). Remind that any intersection means an equilibrium point of the system. Notice that the previous method allowed us to obtain the bifurcation value d_c with a 20 decimal digits precision. This value of d_c will be the one used in all of our analyses carried out with the deterministic model.

3. NUMERICAL SOLUTIONS

The numerical solutions for Eqs. (2)-(3) have been obtained using the 4th order Runge-Kutta method with a constant time step size $\Delta t = 0.1$

4. QUASI-POTENTIAL FUNCTIONS

The stability for many one-dimensional models can be derived from the so-called potential function, U, connected to the dynamical flow through the expression

$$\frac{dx}{dt} = -\frac{dU}{dx}, \tag{4}$$

which gives a formal definition:

$$U(x) = -\int \left(\frac{dx}{dt}\right) dx.$$

It can be shown that the minima and maxima of U correspond to the stable and unstable equilibrium points of the dynamics, respectively. This is in fact the formal expression of the (usually qualitative) pictures where a marble representing the state of the system rolls down from the bottom of one valley to another one as some parameters are changed. This is a well-known picture for physical systems where forces (causing the dynamical trajectories) are derived from energy functions.

The mathematical definition of a potential function for more than one-variable system can be generalised as follows:

$$\tilde{U}\left(\mathbf{x}\right) = -\int \vec{F} d\mathbf{x},$$

$\mathbf{x}$ being an n-dimensional vector state representing the population composition.

The potential energy ($\tilde{U}$) in a point in the phase space space is the energy needed to achieve the minimum energy by dissipation. This approach can have problems when the system has more than one dimension. Moreover, in order to maintain the same definition, the system needs to be conservative. Conservative systems are those accomplishing:

$$\frac{\partial F(x,y)}{\partial x} = \frac{\partial G(x,y)}{\partial y}.$$

If this condition is true, the 2D potential function can be represented as:

$$V\left(x,y\right) = -\left(\int \frac{dx}{dt} dx + \int \frac{dy}{dt} dy\right). \tag{5}$$

In our case, the system is not conservative. This is shown in the difference between the cross derivatives ($d\dot{V}/dS$ and $d\dot{S}/dV$), given by:

$$\frac{\partial}{\partial S}\frac{\partial V}{\partial t} = V(b - cV) \neq f(1-S) - 2V(f + S(b+c)) - m = \frac{\partial}{\partial V}\frac{\partial S}{\partial t}.$$

It is not possible to define a potential function when the system is not conservative. Alternatively, one can use the so-called quasi-potential function, following Eq. (5), which has not a physical potential meaning, but can be used to illustrate the stability of the model. In our system, the integrals of the ODEs are:

$$\begin{aligned}
\int \frac{\partial V}{\partial t} \partial V &= V^2 \left(\frac{Sb - m}{2} - \frac{cSV}{3}\right), \\
\int \frac{\partial S}{\partial t} \partial S &= VS\left(f(1-V) + m\right) + \frac{S^2}{2}\left(cV^2 - bV - d - f\right).
\end{aligned}$$

Then, the quasi-potential function is:

$$\tilde{U}(V,S) = -V^2 \left(\frac{Sb - m}{2} - \frac{cSV}{3}\right) - VS\left(f(1-V) + m\right) - \frac{S^2}{2}\left(cV^2 - bV - d - f\right).$$

In the case that these integrals are not possible to compute, or the underling system of equations is not well defined, there exist ways to approximate the quasi-potential function numerically. This quasi-potential function is related with the orbits of the dynamical system that can be computed numerically from the differential equations (Bhattacharya *et al.* (2011), Qiu *et al.* (2012), Li *et al.* (2013)). We will use the method implemented in Bhattacharya *et al.* (2011), which is based on the following expression:

$$V(x,y) = -\int \left(\left(\frac{dx}{dt}\right)^2 + \left(\frac{dy}{dt}\right)^2\right) dt.$$

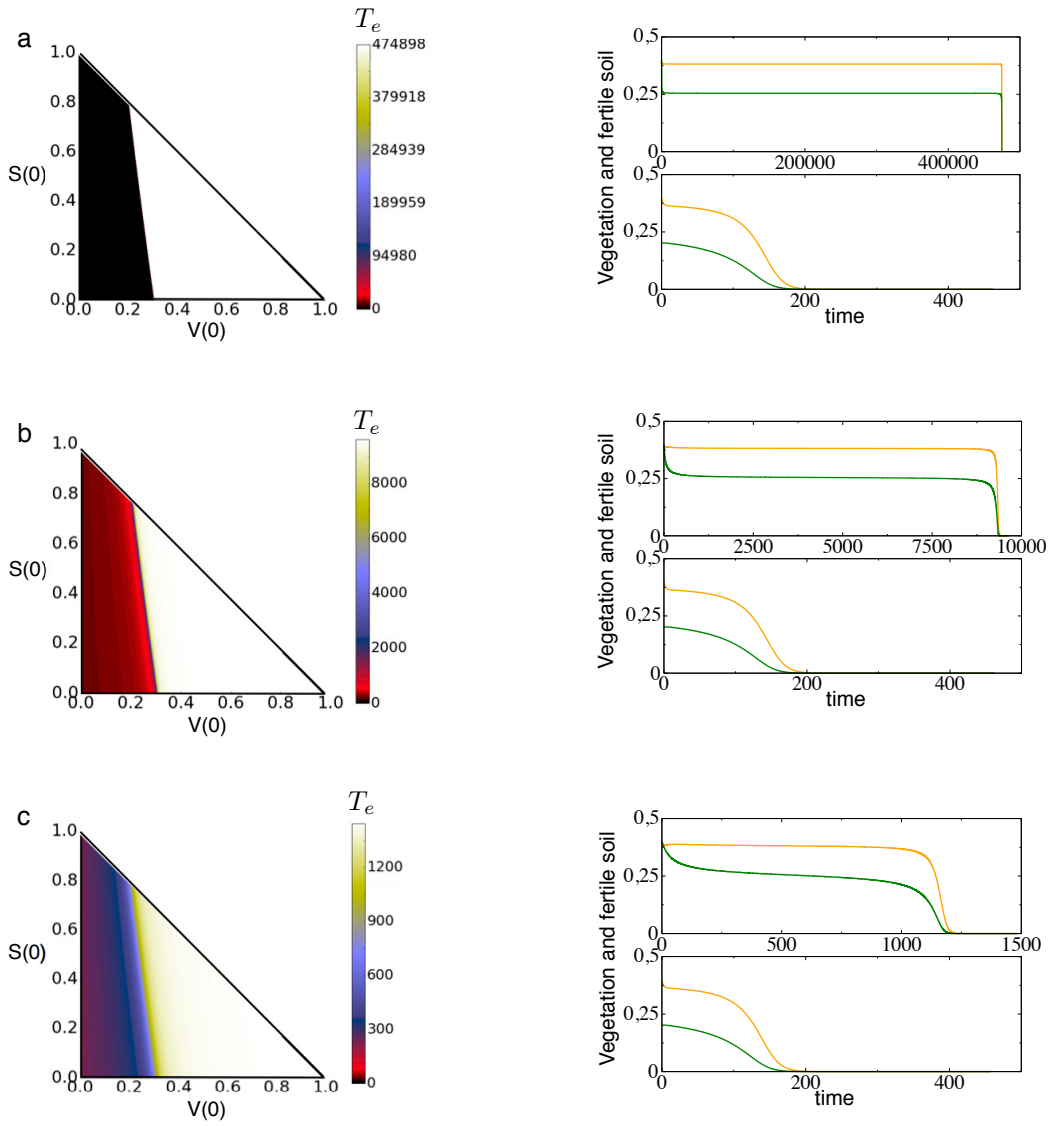

FIG. 3: Extinction times, T_e, computed numerically in the space of initial conditions $(V(0), S(0))$ setting $d \gtrsim d_c$, with: (a) $d = 0.218033995$; (b) $d = 0.21805$; and (c) $d = 0.219$. We also display transients for vegetation (green) and fertile soil (orange) states towards the desert state using two different initial conditions: (upper) initial conditions close to the bifurcation collision point $(V(0) = 0.4, S(0) = 0.4)$; and (lower) initial conditions far away from the collision point $(V(0) = 0.2, S(0) = 0.4)$.

If we take a closer look to this formula, we can see that it is equivalent to the analytical definition:

$$V_{(x,y)} = -\int \left(\left(\frac{dx}{dt}\right)^2 + \left(\frac{dy}{dt}\right)^2 \right) dt = -\int \left(\frac{dx}{dt}\frac{dx}{dt} + \frac{dy}{dt}\frac{dy}{dt} \right) dt$$
$$= -\int \frac{dx}{dt} dx - \int \frac{dy}{dt} dy = -\int \dot{x} dx - \int \dot{y} dy = -\int (\dot{x} dx + \dot{y} dy) = -\int \vec{F} d\mathbf{x}.$$

The numerical computation of the quasi-potential functions is done using the following algorithm:

1. Define a grid of initial conditions. In our case the mesh of initial conditions are from $S_0 = V_0 = 0$ to $S_0 = V_0 = 1$ with $\Delta_S = \Delta_V = 2 \times 10^{-3}$. This defines a 500×500 grid.

2. Compute the solutions of Eqs. (1) by numerical integration until the system reaches the equilibrium. In our case we used $t = 10^9$.

3. Compute the integral for each component, following:

$$U(V_0, S_0) = \left(\sum_{t=1}^{T} V(t) - V(t-1) \right)^2 + \left(\sum_{t=1}^{T} S(t) - S(t-1) \right)^2 .$$

5. NUMERICAL STUDY OF THE INTERVENTION STRATEGIES

In this section we explain how the intervention method has been tested numerically. Two different processes have been considered: (i) increase of the amount of vegetation, labeled ΔV; and (ii) frequency of application of (i). To investigate the impact of the interventions in the system modeled by Eqs (2)-(3) in the main article, we have modified the 4th order Runge-Kutta method to introduce these two processes. Below we display the algorithm (in pseudocode form) used to test computationally the designed intervention method.

Algorithm 1 : Intervention algorithm using a 4th order Runge-Kutta method

set $V_0 = V(0)$ and $S_0 = S(0)$

set $t = 0$

for i *in* $iterations$ **do**

$t = t + \Delta t$

$k_1^{v,s} = \vec{f}(V, S)\Delta t$

$k_2^{v,s} = \vec{f}(V + \frac{1}{2}k_1^v, S + \frac{1}{2}k_1^s)\Delta t$

$k_3^{v,s} = \vec{f}(V + \frac{1}{2}k_2^v, S + \frac{1}{2}k_2^s)\Delta t$

$k_4^{v,s} = \vec{f}(V + k_3^v, S + k_3^s)\Delta t$

if $mod(t, freq) == 0$ **then**

$V_{i+1} = V_i + \frac{1}{6}\left(k_1^v + 2(k_2^v + k_3^v) + k_4^v\right) + \Delta V$

$S_{i+1} = S_i + \frac{1}{6}\left(k_1^s + 2(k_2^s + k_3^s) + k_4^s\right)$

else

$V_{i+1} = V_i + \frac{1}{6}\left(k_1^v + 2(k_2^v + k_3^v) + k_4^v\right)$

$S_{i+1} = S_i + \frac{1}{6}\left(k_1^s + 2(k_2^s + k_3^s) + k_4^s\right)$

Here V_0 and S_0 are the initial conditions; t is time (in arbitrary units); Δt is the constant time step size; $\vec{f}$ is the field (differential equations). The function $mod(t, freq) = 0$ determines the time t at which a given amount of fixed vegetation (ΔV) is introduced at a given frequency, $freq$.

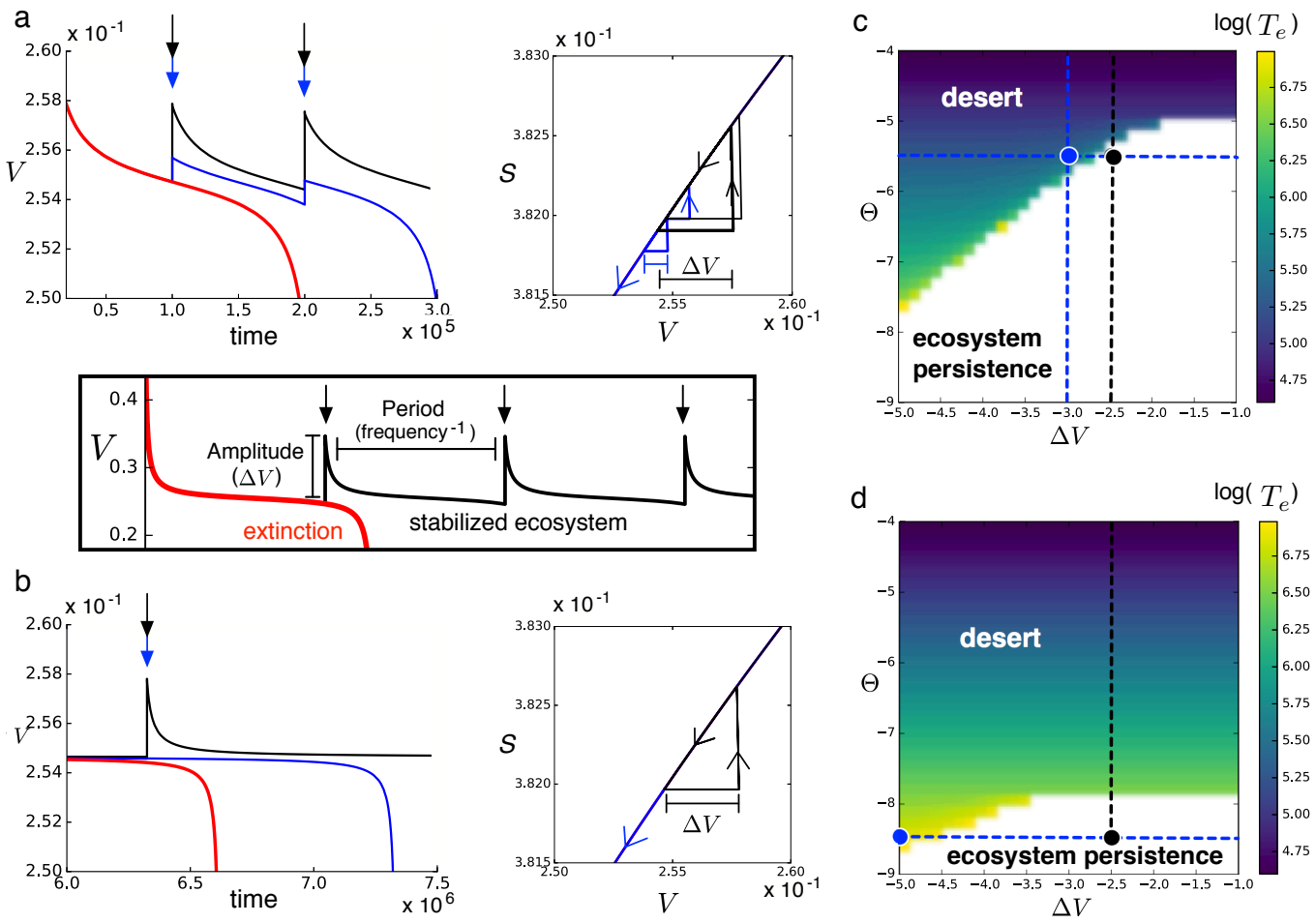

FIG. 4: (a-b) Intervention strategies able to maintain ecosystem's persistence after the bifurcation. The time series in panels (a) and (b) display three different dynamical outcomes beyond the bifurcation: the red trajectory indicates the extinction of the ecosystem without interventions. The blue line indicates an intervention that is not able to preserve the ecosystem; and the black time series corresponds to successful interventions able to preserve the vegetated state. Note that the intervention can be performed by adding a small amount of vegetation (ΔV) at a given frequency (see black rectangle between panels (a) and (b)). The different dynamics can be visualized in the phase space (V, S) for each case. The time series and the orbits plotted in black and blue in panels (a) and (b) correspond to the values indicated in panels (c) and (d) with black and blue circles (and with black and blue dashed lines), respectively. These panels display the the values of ΔV and θ (with $\theta = d - d_c$, shown in log-log scale) involving ecosystem persistence (white area) and extinction (plotting the times towards the desert state (in $\log_{10}(T_e)$) using a frequency of interventions of $freq = 3 \times 10^{-4}$.

Bhattacharya S, Zhang Q, and Andersen ME. (2011) A deterministic map of Waddington's epigenetic landscape for cell fate specification. *BMC Syst. Biol.* **5**, 85.

Ferragut A, García-Saldaña JD, Gasull A. 2015 Detection of special curves via the double resultant. *Qual. Theory Dyn. Syst.* **16**, 101-117.

García-Saldaña JD, Gasull A, Giacomini H. 2014 Bifurcation diagram and stability for a one-parameter family of planar vector fields. *J. Math. Anal. Appl.* **413**, 321-342.

García-Saldaña JD, Gasull A. 2015 Bifurcation values for a family of planar vector fields of degree five. *Discrete Contin. Dyn. Syst.* **35**, 669-701.

Li C, Wang J. 2013 Quantifying Waddington landscapes and paths of non-adiabatic cell fate decisions for differentiation, reprogramming and transdifferentiation. *J. R. Soc. Interface* **10**(89), 20130787.

Qiu X, Ding S, Shi T. 2012 From understanding the development landscape of the canonical fate-switch pair to constructing a dynamic landscape for two-step neural differentiation. *PLoS One* **7**, 12.

Niu W, Wang D. 2008 Algebraic approaches to stability analysis of biological systems. *Mathematics in Computer Science* **1**, 507-539.

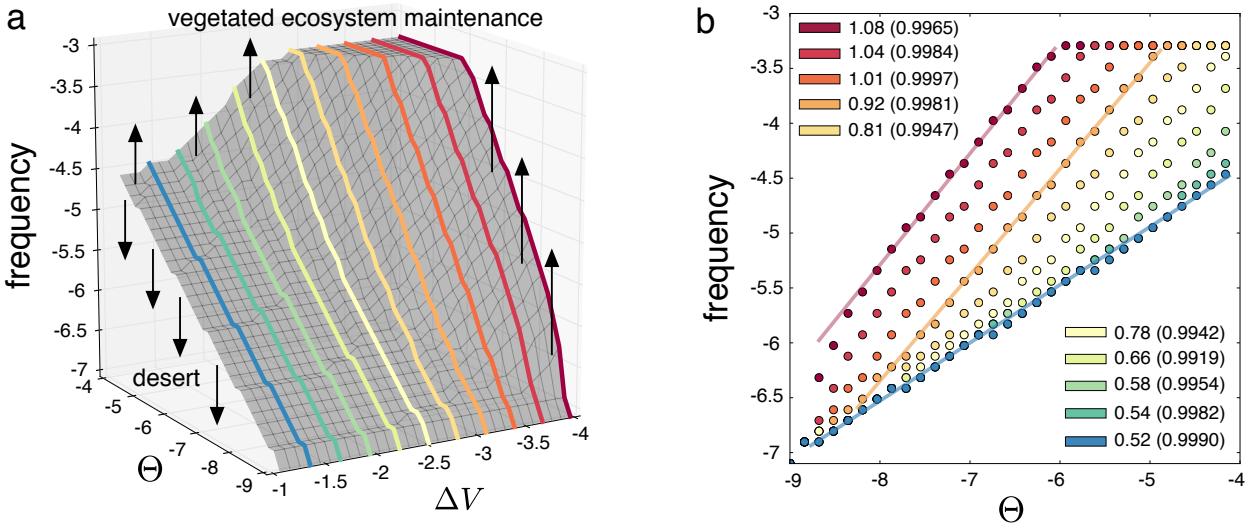

FIG. 5: (a) Surface separating the regions for which the interventions allow to maintain the vegetation (scenario found above the gray surface) and the ones that fail to do so (scenario found below the gray surface). The surface in panel (a) is Pareto optimal: it corresponds to the minimum frequencies and the minimum intervention magnitudes needed for the maintenance of the vegetated ecosystem. (b) Cost increases in terms of frequency depending on Θ i.e., on the distance to the bifurcation value, for different values of ΔV, displayed in panel (a). Depending on the magnitude of the intervention, the frequency needed to hold the vegetation increases with different slopes as d increases beyond the bifurcation value. From red to blue, the frequencies of the interventions increase although the slopes decrease. The straight lines in (b) display three examples of power-law fits. These fits have been performed for all of the cases represented in (b). Inside the plot we display the scaling exponents of these power-law fittings and the values inside the parentheses display the correlation coefficients of these fittings. The values of the other parameters are the same than the ones used in the main article.

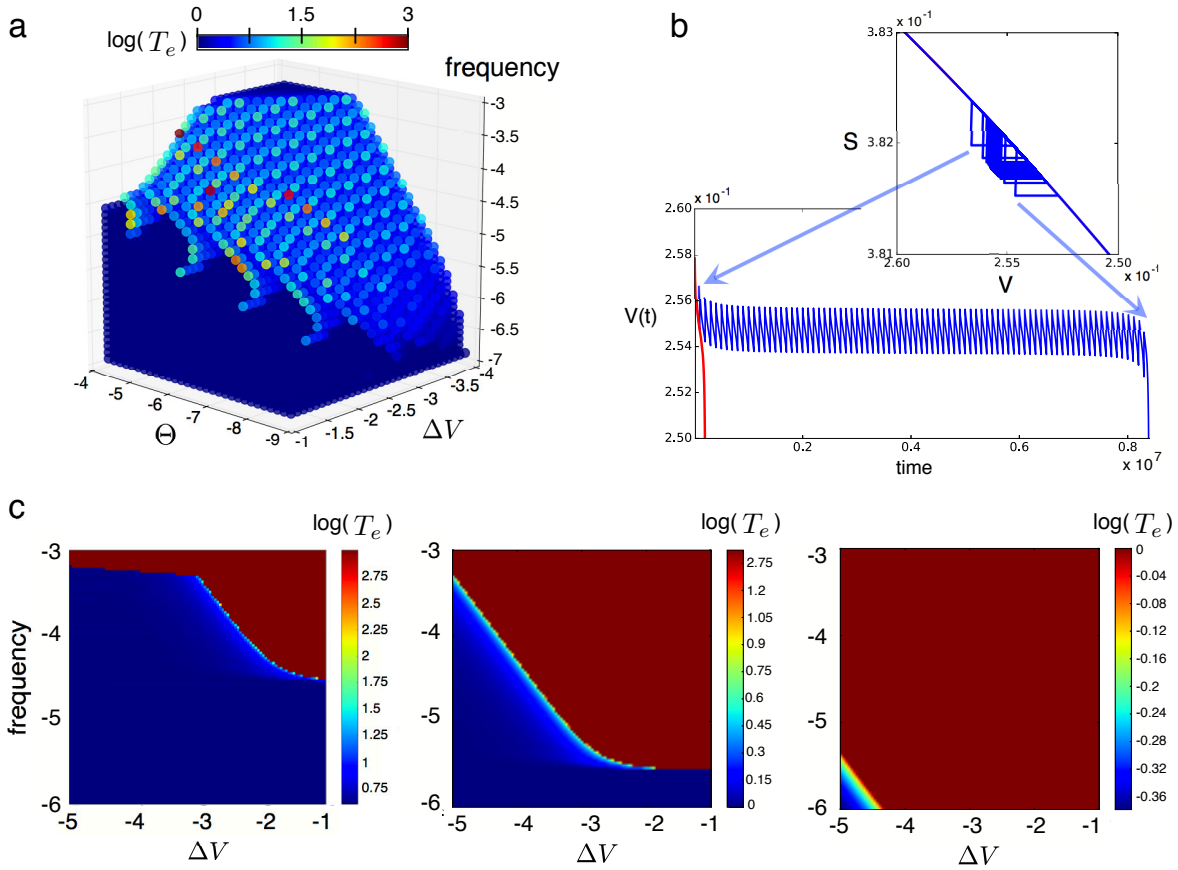

FIG. 6: (a) Increase in the extinction times, T_e (shown in logarithmic scale in the space $(\Delta V, \theta, freq)$), with respect to the non-intervention case in conditions of extinction. An example of an elongation of survival times is illustrated in (b), where the intervention (using $freq = 10^{-5}$ and $\log_{10}(\Delta V) = -2.7127$) increases the time from 2×10^5 (red) to 8.5×10^6 (blue) at $\log_{10}(\Theta) = -5.5$. (c) Increase of T_e depending on the intervention magnitude ΔV and frequency (sampling 100×100 points in the parameter space space $(\Delta V, freq)$). From left to right: $\Theta = 10^{-8}$, $\Theta = 10^{-6}$, and $\Theta = 10^{-4}$. The other parameters are the same used in the previous figures.

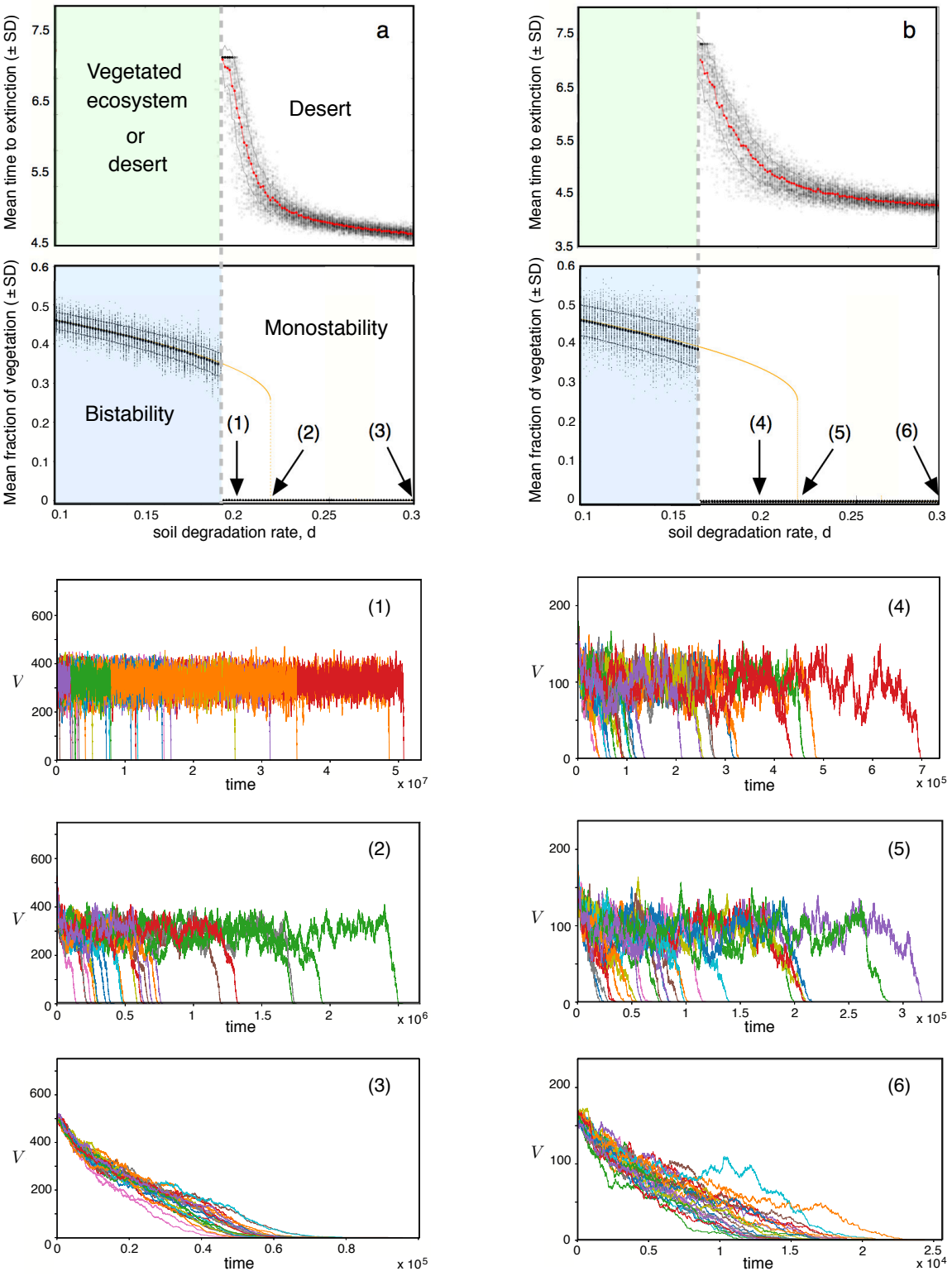

FIG. 7: (a-b) Mean extinction times for vegetation (red line, $\pm$ SD in gray) at increasing soil degradation rate, d, represented in linear-log scale and computed from 100 independent runs. Two system sizes are analyzed: $\mathbb{S} = 10^3$ (a) and $\mathbb{S} = 10^{2.5}$ (b). For the sake of clarity, the bifurcation diagrams computed for the same parameter values using the deterministic (orange) and stochastic (black dots) models are displayed below panels (a) and (b). The vertical dashed lines indicate the stochastic transition value, d_c^s. Below these panels, we display examples of the stochastic dynamics obtained for different values of d in (a) and (b), indicated with numbers, plotting 25 stochastic trajectories in each panel.

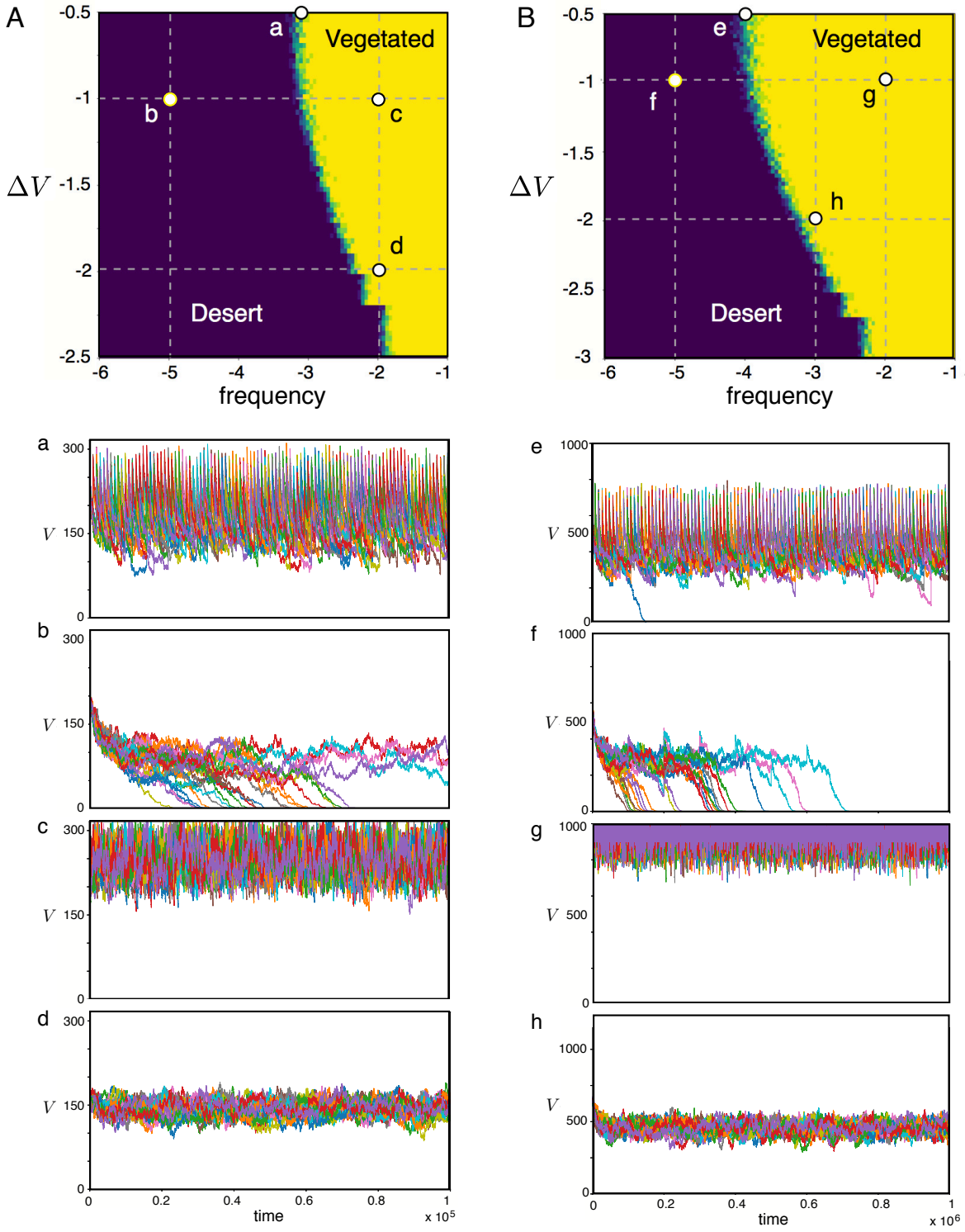

FIG. 8: Impact of the frequencies and of the amount of vegetation replanted on the dynamics of the semi-arid ecosystem under stochasticity using two system sizes: $\mathbb{S} = 10^{2.5}$ (A) and $\mathbb{S} = 10^{3}$ (B). These panels are zooms from the same analyses shown in Fig. 5b and Fig. 5d in the main manuscript. Several intervention dynamics are displayed using 25 overlapped replicates: (a) $\Delta V = 10^{-0.5}$ and $freq = 10^{3.1}$; (b) $\Delta V = 10^{-1}$ and $freq = 10^{-5}$; (c) $\Delta V = 10^{-1}$ and $freq = 10^{-2}$; (d) $\Delta V = 10^{-2}$ and $freq = 10^{-2}$; (e) $\Delta V = 10^{-0.5}$ and $freq = 10^{-3.5}$; (f) $\Delta V = 10^{-1}$ and $freq = 10^{-5}$; (g) $\Delta V = 10^{-1}$ and $freq = 10^{-2}$; and (h) $\Delta V = 10^{-2}$ and $freq = 10^{-3}$.